Photothermal heterodyne holography of gold nanoparticles

E. Absil[1], G. Tessier[1]*, M. Gross[2], M. Atlan[1], N. Warnasooriya[1], S. Suck[1], M. Coppey-Moisan[3] and D. Fournier[1]

[1] *École Supérieure de Physique et de Chimie Industrielles ParisTech, Institut Langevin CNRS UMR 7587 and LPEM CNRS UPR A0005, 10 rue Vauquelin 75231 Paris Cedex 05, France*

[2] *Laboratoire Kastler-Brossel de l'Ecole Normale Supérieure, CNRS UMR 8552, UPMC, 24 rue Lhomond 75231 Paris Cedex 05, France*

[3]*Département de Biologie Cellulaire, Institut J. Monod, CNRS UMR 7592, 2 Place Jussieu, Tour 43, 75251 Paris Cedex 05, France*

**gilles.tessier@espci.fr*

Abstract: We report a method based on heterodyne numerical holography associated to photothermal excitation for full field and three-dimensional localisation of metallic nanoparticles. A modulated pump laser (λ = 532 nm) heats several particles, creating local refractive index changes. This modulation is detected using a probe and a local oscillator beam (λ = 785 nm), frequency-shifted to create a hologram beating at low frequency. Tens of particles, down to diameters of 10 nm, can be localised simultaneously and selectively in three dimensions with near- diffraction resolution by a numerical reconstruction of a single hologram acquired in 5 s.

OCIS codes: (090.1995) Digital holography; (190.4870) Photothermal effects; (180.6900) Three-dimensional microscopy.

References and links

1. C. Sönnichsen, S. Geier, N. E. Hecker, G. von Plessen, J. Feldmann, H. Ditlbacher, B. Lamprecht, J. R. Krenn, F. R. Aussenegg, V. Z. H. Chan, J. P. Spatz, and M. Moller, "Spectroscopy of single metallic nanoparticles using total internal reflection microscopy," Appl. Phys. Lett. **77**(19), 2949–2951 (2000).
2. V. Jacobsen, P. Stoller, C. Brunner, V. Vogel, and V. Sandoghdar, "Interferometric optical detection and tracking of very small gold nanoparticles at a water-glass interface," Opt. Express **14**(1), 405–414 (2006).
3. M. A. van Dijk, A. L. Tchebotareva, M. Orrit, M. Lippitz, S. Berciaud, D. Lasne, L. Cognet, and B. Lounis, "Absorption and scattering microscopy of single metal nanoparticles," Phys. Chem. Chem. Phys. **8**(30), 3486–3495 (2006).
4. A. Arbouet, D. Christofilos, N. Del Fatti, F. Vallée, J. R. Huntzinger, L. Arnaud, P. Billaud, and M. Broyer, "Direct measurement of the single-metal-cluster optical absorption," Phys. Rev. Lett. **93**(12), 127401 (2004).
5. D. Boyer, P. Tamarat, A. Maali, B. Lounis, and M. Orrit, "Photothermal imaging of nanometer-sized metal particles among scatterers," Science **297**(5584), 1160–1163 (2002).
6. A. Rosencwaig, J. Opsal, W. L. Smith, and D. L. Willenborg, "Detection of Thermal Waves through Optical Reflectance," Appl. Phys. Lett. **46**(11), 1013–1015 (1985).
7. S. Berciaud, L. Cognet, P. Poulin, R. B. Weisman, and B. Lounis, "Absorption spectroscopy of individual single-walled carbon nanotubes," Nano Lett. **7**(5), 1203–1207 (2007).
8. D. Lasne, G. A. Blab, S. Berciaud, M. Heine, L. Groc, D. Choquet, L. Cognet, and B. Lounis, "Single nanoparticle photothermal tracking (SNaPT) of 5-nm gold beads in live cells," Biophys. J. **91**(12), 4598–4604 (2006).
9. M. Atlan, M. Gross, P. Desbiolles, E. Absil, G. Tessier, and M. Coppey-Moisan, "Heterodyne holographic microscopy of gold particles," Opt. Lett. **33**(5), 500–502 (2008).
10. F. Dubois, and P. Grosfils, "Dark-field digital holographic microscopy to investigate objects that are nanosized or smaller than the optical resolution," Opt. Lett. **33**(22), 2605–2607 (2008).
11. M. Atlan, M. Gross, and E. Absil, "Accurate phase-shifting digital interferometry," Opt. Lett. **32**(11), 1456–1458 (2007).
12. C. F. Bohren, and H. D.R., eds. *Absorption and scattering of light by small particles* (Wiley, Chichester, UK, 1998).

#116225 - $15.00 USD Received 25 Aug 2009; revised 5 Oct 2009; accepted 15 Oct 2009; published 6 Jan 2010

1. Introduction

The optical tracking of metallic nanoparticles is emerging as an interesting approach in both physical and biological applications, where they offer a photostable alternative to fluorescent labels. Owing to their relatively large scattering efficiency, these markers can be detected directly using dark field or total internal reflection (TIR) illumination [1] down to particle diameters of 40 nm. The detection of smaller objects typically involves interferometric approaches [2,3], or the introduction of an additional modulation [4]. One of the most sensitive and selective techniques, scanning photothermal heterodyne detection [5] actually combines interferometric detection and photothermal modulation to discriminate particles smaller than 5 nm from their background.

Photothermal excitation is a well established technique for the sensitive detection of absorbing objects. A modulated optical beam is sent on the sample, creating a localised heating, which in turn induces a variety of phenomena including e.g. infrared emission, thermal expansion, or refractive index changes [6]. When detected with good sensitivity, these phenomena can deliver information on the optical absorption of the sample. Recently, these techniques have been adapted to the detection of metal nanoparticles [5] or nanotubes [7], specially in the context of biological studies [8]. Relying on absorption, which scales as the volume of the particle, rather than scattering, which varies as the square of the particle volume, is clearly an advantage for the detection of very small particles. Most techniques so far use single-point measurements, and the lack of fast full field imaging can be partially circumvented by tracking a particle while it is moving [8]. Assemblies of beads can also be imaged, provided that their displacement and the temporal noises, which translate into spatial noises, are negligible during the scan. However, wide field detection, which would certainly be of great interest in most applications, can only compare to single point detection in terms of sensitivity if an interferometric imaging technique is used [9,10].

We propose here a wide field, CCD-based heterodyne holography technique, which is able to achieve three dimensional imaging of gold nanoparticles submitted to a modulated photothermal excitation. Heated nanoparticles induce a temperature modulation and a small refractive index variation (10^{-3} to 10^{-5} K^{-1}) in the surrounding medium. This relatively large heated region scatters light towards the camera, where it interferes with a phase-shifted reference beam. The reconstruction of this hologram is then obtained numerically [9].

2. Experimental setup

The setup described in Fig. 1 is devised around a commercial BXFM Olympus microscope, which is extremely useful to carry out visual examinations of the samples. Dark field and interferential contrast modes, which are helpful in biological contexts, are readily usable on the system. The holographic arms use a single mode laser diode beam emitting around 50 mW at $\lambda = 785$ nm. A half wave ($\lambda/2$) plate associated to a polarizing beam splitter (PBS) is used to distribute the intensity between the reference (optical electric field E_R) and illumination (E_I) beams, in addition to neutral density filters (ND1 and ND2), so that most of the available light (typ. 90%) illuminates the object. Both beams are frequency-shifted by acousto-optical modulators (AOM) at frequencies F_{AOM1} and F_{AOM2} around 80 MHz. To align the polarization of both beams and allow interference, one of the beams passes through a half wave plate. It then illuminates the sample through a prism in dark field configuration. The scattered field is collected by a microscope objective (x100, N.A. = 0.8) and reaches the camera where it interferes with an expanded reference beam forming an angle $\theta \approx 1°$ with respect to the optical axis. Since both beams are frequency-shifted at F_{AOM1} and F_{AOM2}, the interference pattern resulting from this off-axis optical mixing is modulated at a beating frequency $\Delta F = F_{AOM1} - F_{AOM2}$, which can be low enough to allow measurements with a slow detector. Here, these fringes are recorded by a CCD camera (Roper Cascade 512 F, frame transfer 512x512, 16x16 µm pixels matrix, triggered at a frame rate F_{cam} = 16Hz). Like most heterodyne interferometers, this setup allows the investigation of phenomena modulated at any frequency F_{inv} by choosing the appropriate detuning ΔF, so that $F_{inv} = \Delta F \pm F_{cam}/k$, where the sign

#116225 - $15.00 USD Received 25 Aug 2009; revised 5 Oct 2009; accepted 15 Oct 2009; published 6 Jan 2010

determines the position of the direct (order 1) and twin (order −1) images in the reconstruction [11], and k≥2 is an integer (k = 4 in our case). A direct holographic imaging of metallic particles has already been demonstrated [9,10] in the static case $F_{inv} = 0$.

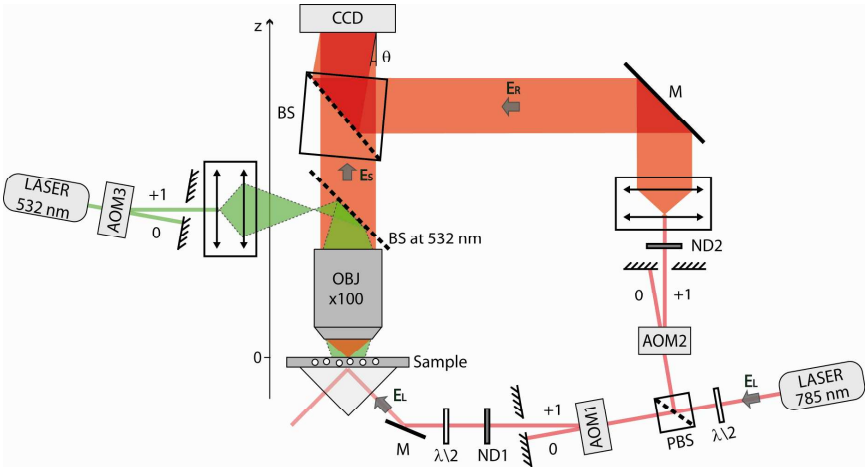

Fig. 1. Experimental setup. AOM: Acousto-Optical Modulators. ND: Neutral Density filters. PBS and BS: Polarizing (resp. non-Polarizing) Beam Splitter. M: Mirror.

Here, the photothermal excitation is delivered by a 2W, continuous multimode solid state laser at λ = 532 nm, which is sine-modulated by AOM3. Unlike AOMs 1 and 2, it serves as a heating power modulator by using a 80 MHz carrier, modulated in amplitude at F_{AOM3}. This beam is directed into the objective by a dichroïc beamsplitter (BS at 532 nm). An adjustable beam expander slightly uncollimates the beam to illuminate a 2 µm to 200 µm diameter region of the sample. At high laser power, an additional notch filters ensures that no heating light reaches the camera. This excitation, when hitting a point-like object in a homogeneous medium, creates a spherical region in which the temperature is modulated. A local modulation of the refractive index appears in this heated region due to photothermal effects, and is investigated by synchronizing the setup to $F_{inv} = F_{AOM3}$.

The samples are thin spin-coated layers of gold beads (diameters 10 to 100 nm) immobilized in a Poly Vinyl Alcohol (PVA) matrix and covered with a thin layer of paraffin oil which allows a correct heat diffusion and acts as a photothermal medium. Under holographic examination, all particles appear to be in the same plane, indicating that the thickness of the PVA film is below the axial resolution of the technique, and that most particles are therefore in contact with the glass substrate. This glass slide is optically coupled to the TIR prism using index matching oil, so that the reflection occurs at the interface between PVA and air, creating an evanescent wave which is locally frustrated and scattered to the far field by gold beads, photothermal modulation, or imperfections. Note that PVA/liquid interfaces are not adapted to TIR, forbidding the use of immersion optics in this configuration.

3 Experimental results

3.1 Direct and photothermal holography of 50 nm beads

Figure 2 presents a comparison of direct and photothermal images of the signal $|E_S.E_R^*|^2$ in the same region of a 50 nm beads sample reconstructed after demodulation, spatial filtering in the Fourier space, and numerical propagation to the object plane [11]. The reconstruction is carried out with a 2-FFT algorithm, over 512x512 pixels. Direct holography (Fig. 2a) was obtained without heating, for ΔF = 4 Hz, sampled by the camera at a rate $F_{cam} = 4\Delta F = 16$ Hz. Photothermal holography (Fig. 2b and 2c) was carried out at a heating modulation frequency F_{AOM3} = 5 kHz, with ΔF = 5 kHz + 4 Hz, and again F_{cam} = 16 Hz, with an average power of 210 mW reaching a 180 µm^2 region of the sample (dashed circle in Fig. 2), for a mean power

#116225 - $15.00 USD Received 25 Aug 2009; revised 5 Oct 2009; accepted 15 Oct 2009; published 6 Jan 2010

density of 120 kW.cm^{-2}. In both cases, 48 images were accumulated, with an integration time of 100 ms each, for a total acquisition time of 5s. In Fig. 2b, only the heated particles are visible, confirming that a photothermal phenomenon is actually being observed.

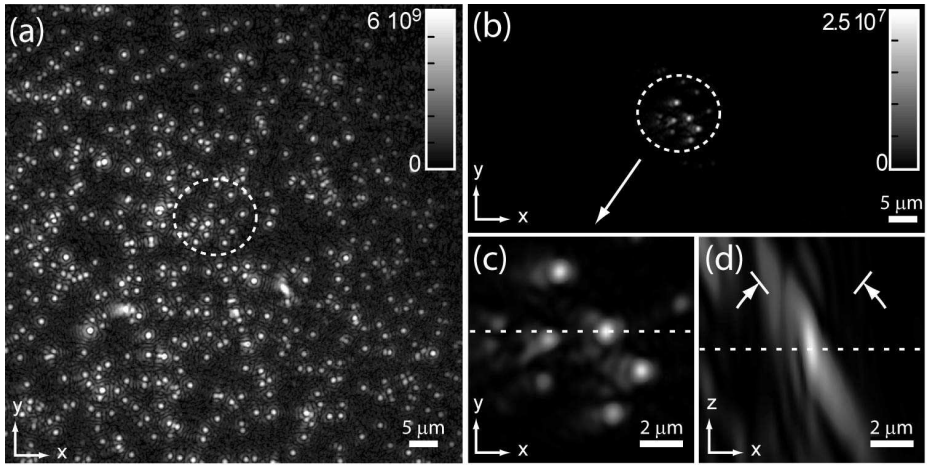

Fig. 2. (a) Holographic intensity image ($|E_S.E_R^*|^2$, arb. units) of 50 nm gold particles embedded in PVA, 512 x 512 pixels. (b) photothermal reconstructed hologram (512 x 210 pixels) of the same sample heated up by a λ = 532 nm, 210 mW average power laser modulated at 5 kHz (dashed circle). (c) Central region of the same image (67x67 pixels, interpolated to 670x670 pixels for clarity). The dashes represent the plane of (d): reconstruction along a plane perpendicular to the sample obtained with the same hologram, 62x62 pixels. The arrows materialize the collection angle of the microscope objective.

3.2 Three-dimensional reconstruction

A single hologram allows the calculation of the amplitude scattered by the photothermal objects in virtually any z- plane to obtain a 3D stack of images. Most photothermal objects have similar characteristics. Figure 2d presents a cross section in a stack calculated with steps of Δz = 90 nm (equivalent of the size of the pixels in the image plane), showing the field scattered by relatively isolated photothermal objects in a plane perpendicular to the sample. It is mostly oriented along the direction of the incident light, close to the maximal acceptance angle of the microscope objective, 38°, which was measured in an independent experiment. This complex shape reflects the portion of the light which is mostly scattered forward by the relatively large hot region and is effectively collected by the microscope objective. In the (x,y) plane, the photothermal objects have a 1/e diameter of the order of 0.9 µm for F_{AOM3} = 5 kHz. This size is above the diffraction limit, 590 nm for this objective, and is related to the thermal diffusivity of the surrounding medium. An order of magnitude calculation for this diffusivity yields $D_{eff} = \pi.F_{AOM3}.\mu_{eff}^2 = 4 \times 10^{-9}$ m^{2}s^{-1}, smaller than the diffusivity of oil, $D_{oil} = 8 \times 10^{-8}$ m^{2}s^{-1}.

To validate the photothermal origin of the signals, we carried out a study of the heating power density dependence of the photothermal signal. In this holographic system, the signal is given by the interference term $E_S.E_R^*$, where the scattered amplitude E_S is proportional to the polarization $\vec{P}(\vec{r},t)$ induced at a distance $\vec{r}$ from the particle by the incident field $E_L(\vec{r},t)$:

$$\vec{P}(\vec{r},t) = \varepsilon_0 \frac{\Delta\chi(\vec{r},t)}{n^2} E_L(\vec{r},t) \qquad (1)$$

where $\Delta\chi(\vec{r},t)$ is the local susceptibility variation [12]. In the case of a particle absorbing a fraction C_{abs} of the incident heating power density P_{Heat}, the local susceptibility variation is:

#116225 - $15.00 USD Received 25 Aug 2009; revised 5 Oct 2009; accepted 15 Oct 2009; published 6 Jan 2010

$$\Delta\chi(r,t) = 2n\frac{\partial n}{\partial T}\Delta T(r,t) = 2n\frac{\partial n}{\partial T}\frac{C_{abs}P_{Heat}}{4\pi\kappa r}\left[1+e^{-\frac{r}{\mu}}\cos\left(2\pi F_{AOM3}t-\frac{r}{\mu}\right)\right] \qquad (2)$$

where κ is the thermal conductivity of the surrounding medium and μ is the thermal diffusion length. It follows directly from (1) and (2) that $|E_S.E_R^*|$ is directly proportional to the heating power P_{Heat}, and the holographic intensity $|E_S.E_R^*|^2$ to P_{Heat}^2. Figure 3 presents an analysis of the photothermal holographic signal obtained for a heating modulation frequency F_{AOM3} = 5 kHz. The heating power density was varied from 17 kW.cm^{-2} to 305 kW.cm^{-2}, keeping the illuminated area constant while changing the optical power. The holographic intensity $|E_S.E_R^*|^2$ from single 50 nm particles was integrated over a distance μ from the center of the particle. Figure 3 presents the variations of the square root of this signal, $|E_S.E_R^*|$. As expected, $|E_S.E_R^*|$, is proportional to the heating power density P_{Heat}, doubling for every 91 W.cm^{-2}, and confirming the photothermal origin of the observed signals. The data of Fig. 3 exhibit fluctuations from a linear behavior, which we interpret as related to variations in the heating laser power which is not actively stabilized.

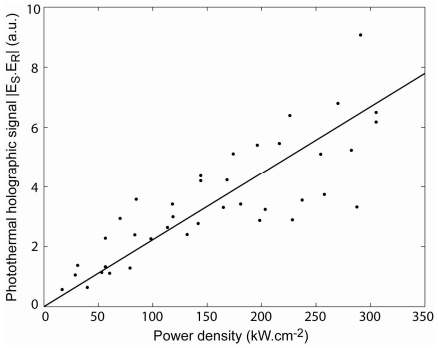

Fig. 3. Power density dependence of the photothermal holographic signal $|E_S.E_R^*|$ (a.u.) from a single 50 nm particle, averaged over pixels located in the vicinity of the particle, for a heating frequency F_{AOM3} = 5 kHz.

3.3 Photothermal holography of 10 nm beads

To illustrate the sensitivity of the setup, we have then imaged samples of 10 nm particles in PVA. In order to compensate for the drastically decreased absorption cross section of such small particles, the 305 mW average power heating beam was focused over a smaller region, only 5 μm in diameter, for a power density of 1.5 × 10^{10} W.m^{-2}. Again, intensity images ($|E_S.E_R^*|^2$) were reconstructed in several planes to obtain the (x,y) and (x,z) sections presented in Fig. 4a and 4b. In the (x,y) plane, the photothermal signal has a nearly diffraction–limited size, indicating that the diameter of the thermal sphere is smaller than 798 nm.

The consistency of the signal levels has been checked by comparing the photothermal signals at different particle sizes, as shown in Fig. 4c for 50 nm and 10 nm particles. While the signal level is higher in direct holographic measurements, the Signal-to-Noise Ratio (SNR) is higher in photothermal holography, owing to a strong reduction of the background and noise levels. The ratio of the signals $S = |E_S.E_R^*|^2$ obtained on 50 nm and 10 nm particles is S_{50nm}/S_{10nm} = 66. This figure can be compared to theoretical expectations. The absorption scales with the power density P_{heat} (with P_{heat} = 120 and 1550 kW.cm^{-2} resp.) and with the 3rd power of the particle diameter, d^3 (with d = 50 and 10 nm resp.), while our signal S scales as the square of the absorption i.e. $P_{heat}^2\ d^6$. The ratio of the signals which is theoretically expected for 10 nm and 50 nm particles is thus $S_{50nm,th.}/S_{10nm,th.} = (120/1550)^2\ 5^6 = 93$. Considering the particle size distribution and likely variations in the heating power, this is a good agreement, confirming that we are indeed detecting 10 nm particles.

#116225 - $15.00 USD Received 25 Aug 2009; revised 5 Oct 2009; accepted 15 Oct 2009; published 6 Jan 2010

On 50 nm particles, the photothermal signal is 133 times lower than the direct signal, as shown in Fig. 4c. However, since the noise is reduced by a factor of 3.4 10^4, the photothermal experiment increases the SNR by a factor of 256. It can be noted in the profiles as well as in the images that some scattering particles which are visible in the direct hologram do not absorb, and do not appear in the photothermal image. On the 10 nm particles, the SNR calculated from a single profile is 90. An overall detection SNR, obtained by integrating the signal from one particle over a disc of radius of 1 µm, and dividing it by an integration of the noise over an identical area, yields a SNR of 5400. In samples able to withstand strong excitation powers, even smaller particles could probably be detected by increasing the heating power. As seen in reconstruction planes not centred on the particle itself (media 1), other large particles (dust or aggregates) can be detected in other planes. The shape of their diffusion pattern (frames 0-20), however, differs strongly from that of the heated particle (frames 80-100): parasitic particles with high refractive index contrast scatter light in several directions, while low index contrast thermal spheres mostly produce a forward diffusion which is a clear signature of gold particles photothermal detection.

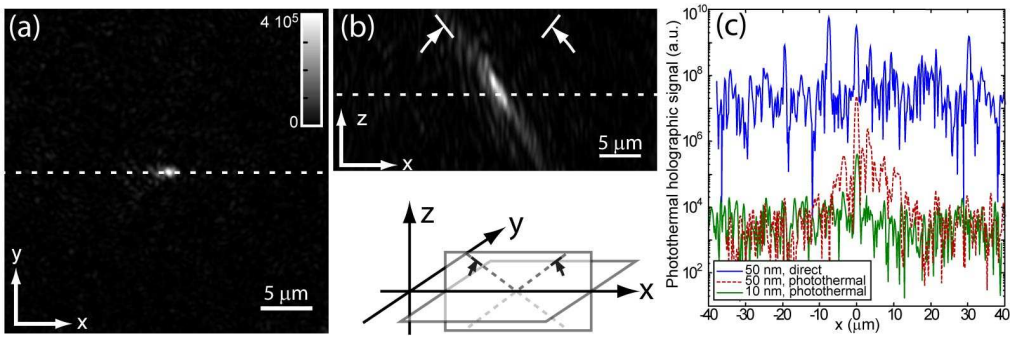

Fig. 4. (a): 200x200 pixels photothermal holographic ($|E_S.E_R^*|^2$, arb. units) image of a 10 nm particle heated by a 305 mW beam modulated at 5 kHz and focused o a 5 µm FWHM disc (power density 1.5 MW.cm^{-2}). (b) reconstruction of the same hologram in the (x, z) plane along the same dotted line, 250x125 pixels, showing the 3D shape of the scattered light. (Media 1) shows the reconstruction in different planes, with steps of 1 voxel (156 nm) between images. The arrows materialize the collection angle of the microscope objective. (c) Log scale profiles of the signal obtained by direct (blue) and photothermal (red dotted line) holography on 50 nm particles at the same position, *i.e.* along the dotted line in Fig. 2c. In green, log profile along the dotted line in 4a) for 10 nm particles. The x axis is centred on the particle under study. One can note that background noise levels are the same for 10 and 50 nm beads photothermal curves.

4 Conclusions

Photothermal heterodyne holography provides an enhancement of the signal/background ratio (see Fig. 4c) by several orders of magnitude compared to direct holography, even for moderate heating power densities. Among the subwavelength particles which cannot be eliminated by visual observation, metallic nanoparticles typically display a much stronger absorption, making the photothermal technique extremely selective with respect to dust or contaminations. This is however obtained at the price of a reduction of the imaged field, to obtain sufficient heating power densities. With an imaged surface of 180 µm^2 obtained in 5 s, photothermal numerical holography is still much faster than scanning-based techniques, which are typically able to image surfaces of 25 µm^2 in more than one minute. Nevertheless, single point scanning photothermal interferometry can still achieve one order of magnitude higher SNRs for identical heating power densities. Imaging a large field with high heating power density requires a high total laser power, which cannot be withstood by delicate samples. The 3D study of the diffusion pattern of individual particles or heated particles is of great interest since it allows an effective discrimination using the shape of diffusion diagrams. Its main advantages, however, are to be found in applications which require the real time, three dimensional imaging of individual nanolabels, notably in biological applications.

#116225 - $15.00 USD Received 25 Aug 2009; revised 5 Oct 2009; accepted 15 Oct 2009; published 6 Jan 2010

Acknowledgement

The authors would like to acknowledge financial support from the Agence Nationale de la Recherche, ANR 3D NanoBioCell and ANR EThNA.

#116225 - $15.00 USD Received 25 Aug 2009; revised 5 Oct 2009; accepted 15 Oct 2009; published 6 Jan 2010